# MODELS OF BIOLOGICAL AGGREGATION

BENJAMIN PITTMAN-POLLETTA

Contents



## 1. Introduction

Social behavior is ubiquitous in the biological world. Birds of a feather flock together - and so do living things at nearly all other levels of complexity. In addition to flocks of birds, herds of mammals, swarms of insects, schools of fish, and even aggregations of bacteria such as slime mold slugs are well-known biological phenomena. Understanding aggregative behaviors is important in many fields of biology, especially ecology and evolution. Recently, mathematical models of biological aggregation have received a lot of attention. Modeling has allowed analogies with other fields have be drawn, and most of these models proposed exhibit coarsening dynamics - a mathematical phenomenon of interest in its own right.

Coarsening dynamics, in which a continuous or discrete density resolves into small, localized clumps which then merge into larger clumps over time, occur in a wide variety of systems. In addition to biological aggregation, this type of behavior is observed in the gravitational interactions of particles in a viscous medium, and in the formation of large water droplets from smaller ones on a dewetting surface. A common characteristic of systems exhibiting coarsening phenomena is the presence of both attractive and diffusive forces, operating on different time and length scales, and with different nonlinear dependence on the underlying density field.

In this paper, I investigate a simple discrete model of chemotactic aggregation which exhibits coarsening dynamics. In this model, a population of

*Date*: November, 2005.

bacteria is represented as a number of small masses, each of which moves as a unit. When two masses come close enough to each other, they merge into a new mass. The way the number of masses scales with time is explored. The dependence of the dynamics on the geometry and statistics of the initial distribution is also investigated, and a possible connection to Laplacian growth is postulated.

The paper is organized as follows. The first section contains a short review of some results on continuum models of biological aggregation, including Keller and Segel's seminal paper on chemotaxis in slime molds. This section also includes summaries of a recent paper by Topaz et al. on a biologically realistic model of swarm formation, and of a paper by J.J.L. Velazquez in which a discrete model of aggregation is seen to be the asymptotic limit of a continuum model much like the Keller-Segel model. The second section discusses the discrete model of biological aggregation explored in this paper, and some numerical results and dimensional analysis for that system. A discussion of these results follows.

## 2. Background

2.1. **The Keller-Segel Model.** Slime molds are single-celled organisms that come together during reproduction to form a multicellular fruiting body that releases a number of spores. (Spores are cells with a hardened exterior which can survive harsh conditions, remaining dormant until conditions improve, when they 'hatch' or germinate.) Cellular slime molds, or dictyostelids, are a type of slime mold that exhibit an unusual life cycle. After germinating and for as long as food is available, slime molds roam the earth as single-celled amoeba. However, when food becomes scarce, these amoeba begin to aggregate to form multicellular 'slugs,' which migrate as a single organism with a definite front and rear end, finally forming a fruiting body. It is known that the aggregation of dictyostelids is mediated by the release of a chemical known as acrasin, which every amoeba produces under the correct conditions.

In 1970, Keller and Segel introduced a continuum model of aggregation in slime molds [1]. This was one of the first mathematical models to describe biological aggregation, and it has since been studied extensively and considerably generalized in the study of other aggregative phenomena. The model attempts to describe the formation of slime mold slugs as the result of the amoebas' ability to sense the acrasin gradient, as opposed to the presence of a 'center' cell. Parameters of the amoeba population which are assumed to vary include the rate of acrasin production, the rate of acrasin breakdown, and the sensitivity of amoeba to acrasin.

The slime mold population density is given by a continuous function on the plane evolving in time - $u(x, y, t)$. The concentration of acrasin, the chemical which causes chemotaxis in slime mold amoeba, is described by the function $c(x, y, t)$. The flux in $u$, the bacterial population density, is accounted for by two forces. The first is random motion, which introduces a diffusive term into the equation. The second is chemotaxis, which is accounted for by movement of bacteria in the direction of $-\nabla c$. Thus,

$$u_t = \nabla(f(u,c)\nabla u) - \nabla(g(u,c)\nabla c), \tag{1}$$

where $f$ and $g$ are positive functions of $u$ and time, representing the propensity of the amoeba to random movement, and the strength of the chemotactic response, respectively. The change in the concentration profile of acrasin is accounted for by diffusion, production by the amoeba, and breakdown by other chemicals released by the amoeba and in the environment:

$$c_t = a\Delta c + h(c)u - j(c)c, \tag{2}$$

where $a$ is a positive constant, and $h$ and $j$ are positive functions of $c$.

The resulting system has a constant steady state $(u_0, c_0)$, corresponding to a uniform distribution of amoeba. Linearizing around this steady state, Keller & Segel discover that it is unstable to periodic perturbations under certain sets of parameters. The instability condition is

$$\frac{c_0 g(u_0,c_0)}{a_0 f(u_0,c_0)} + \frac{u_0 h'(c_0)}{j(c_0)} > 1.$$

The first term above reflects the balance between the tendency of the amoeba to move (represented by the denominator) and the degree to which amoeba are attracted by acrasin. The second term will be larger than one if a small increase in acrasin level causes an increase in acrasin output which outweighs its more rapid decay. These findings are supported by experiment, which show that both sensitivity to acrasin and its production rate rise 100-fold during a period spanning the onset of aggregation.

Finally, it is suggested that a superposition of spatially periodic perturbations with nonparallel wave vectors may give rise to polygonal patterns resembling the clumping solutions observed experimentally.

One weakness of the Keller-Segel model is that at long times, depending on the form of the acrasin-response coefficient $f$, the model exhibits finite time blowup. The model places no bounds either on how fast bacteria can move or on how densely they can inhabit a given region, and so the entire bacterial population becomes concentrated in a single point, a $\delta$-function like mass scaled by

$$M = \int_{-\infty}^{\infty}\int_{-\infty}^{\infty} u(x,y,t)dxdy = \int_{-\infty}^{\infty}\int_{-\infty}^{\infty} u(x,y,0)dxdy.$$

This finite-time blowup is not a characteristic of the physical system.

2.2. **Swarming.** Since [1], attempts have been made to use similar models to describe biological aggregation more accurately and generally. As a case study, I will describe a recent paper [2] analyzing a general but biologically realistic continuum model of aggregation.

Topaz et al. describe a model in which a continuous population density $u$ defined on a domain $D \subset \mathbb{R}^n$ moves in a density-dependent manner with velocity given by the vector field $\mathbf{v}$:

$$u_t + \nabla \cdot (u\mathbf{v}) = 0.$$

The velocity vector $\mathbf{v}$ has two components: an attraction term and a repulsion term. The repulsion term, $\mathbf{v}_r$, due to overcrowding, is local, away from the gradient of the population density, and stronger when the population density is higher.

$$\mathbf{v}_r = -c_r u \nabla u.$$

The strength of the repulsion is measured by the constant $c_r$. The attraction term, $\mathbf{v}_a$, is nonlocal. Each organism is attracted to areas of high population density, and detects population density by sense data in some modality. The effective range of this sensory modality is incorporated into a sensing kernel $K$. The population density detected by each organism is thus a real-valued function on $D$, given by the convolution $K * u$. Organisms move up the gradient of the detected density, and so

$$\mathbf{v}_a = c_a \nabla (K * u),$$

where $c_a$ represents the strength of the attraction. After rescaling, $u$ is seen to satisfy the dimensionless equation

$$u_t + \nabla \cdot [u(\nabla (K * u) - du\nabla u)] = 0, \tag{3}$$

where $d$ is a dimensionless parameter represending the ratio of attractive to repulsive forces. The Keller-Segel model has as sensing kernel the fundamental solution to Laplace's equation; in two dimensions, $K(x) = -\frac{1}{4\pi}\log(|x|)$.

Regardless of the form of the sensing kernel, this equation possesses steady-state solutions and a Lyapunov functional, or energy,

$$E(u) = \int_{\mathbb{R}^2} \left( \frac{r}{3} u^3 - uK * u \right) dx.$$

Next, Topaz et al. perform an in depth analysis of the system (3) for the particular choice of sensing kernel

$$K(x) = K_1^e(x) = e^{-|x|}. \tag{4}$$

$K_1^e$ is called the constant hazard function, and it represents the biologically reasonable assumption that the rate of transmission failure of sensory data per unit distance is constant. System (3), (4) can be defined on a one-dimensional periodic domain $[0, L]$ by noting that $K_1^e = (I - \partial_x^2)^{-1}$. The steady state version of (3), (4) can be rewritten

$$u_x = duu_x - d(uu_x)_{xx}, \qquad x \in \mathbb{R}.$$

This system's solutions include constant steady states, periodic solutions with amplitude inversely proportional to $d$, and compactly-supported solutions which have infinite slope at the boundary and correspond to swarms.For each value of $M$, there is a one-parameter family of swarm solutions. Only one member of each family is observed numerically, and Topaz et al. show that the profile chosen is the one minimizing the system's associated energy. Simulations in one and two dimensions reveal coarsening dynamics as the system evolves towards swarm solutions.

A bifurcation diagram for the system is constructed numerically. As the total mass of the population decreases, constant steady-state solutions corresponding to a uniform distribution of organisms destabilize, and periodic solutions are observed. At $M_c = 3.52$, a periodic solution which has zero density at one point in the domain is observed. As $M$ is further decreased, the support of this 'touchdown periodic' solution shrinks, and swarm solutions are observed. The transition from periodic to swarm solutions is hysteretic. That is, as the total mass of the population increases above $M_c$, swarm solutions may persist.

Finally, Topaz et al. investigate swarm solutions on an unbounded domain by simulating the periodic system in the limit as $L$ approaches infinity. They discover that the system selects a one-parameter family of swarm solutions indexed by total mass. Surprisingly, the maximum density of these solutions is constant. Using energy arguments, it is shown that the maximum density to which organisms aggregate is $u_{max} = 1.5d$, and so related to the balance between attractive and repulsive forces. It is interesting to note that the density dependent repulsion in this sytem causes a density saturation which leads it to avoid the blowup observed in the Keller-Segel model.

2.3. **Discrete Model as Asymptotic Limit.** Some recent work has been devoted to attempts to normalize the Keller-Segel model, in order to remove the unphysical finite-time blowup. One attempt by J.J.L. Velazquez ([3],[4]) uses asymptotic methods to describe the dynamics of the system after blowup using equations for the movement of $\delta$-function like point masses called concentration regions. The system Velazquez intends to describe asymptotically is

$$u_t = \Delta u - \nabla(u\nabla c), \qquad u \in \mathbb{R}^2, \qquad t > 0, \tag{5}$$
$$\Delta c + u = 0.$$

Velazquez first examines a system which does not exhibit finite time blowup - in the term describing the negative gradient motion of the bacteria, $u$ is replaced with $f_\epsilon(u)$, where $f_\epsilon$ is a function approaching $u$ as $\epsilon$ approaches zero:

$$u_t = \Delta u - \nabla(f_\epsilon(u)\nabla c),$$
$$\Delta c + u = 0.$$

For $\epsilon > 0$, this system exhibits solutions which are global in time. In particular, there is an uncountable family of radial steady-state solutions, indexed by their total mass, $M \in [8\pi, \infty)$, which have their mass concentrated in regions of size $\sqrt{\epsilon}$ about the origin. Velazquez assumes that, near blowup, the population density profile consists of a finite sum of such steady-state solutions, which he refers to as concentration regions or singular regions. Outside of these regions, the population density profile can be approximated as a sum of $\delta$-function like contributions from the concentration regions, which are described by their mass $M_j$ and position $x_j$, and a much smaller background density, $u_{reg}$:

$$u \approx \sum_{j=1}^{N} M_j(t)\delta(x - x_j(t)) + u_{reg}. \tag{6}$$

The corresponding acrasin density, which is the solution to Poisson's equation with $u$ as a forcing term, can be approximated as

$$v(x,t) \approx -\frac{1}{2\pi}\sum_{j=1}^{N} M_j(t) log(|x - x_j(t)|) + v_{reg}(x,t), \text{ where}$$

$$v_{reg}(x,t) = \int_{\mathbb{R}^2} \log(|x-y|) u_{reg}(y,t) d^2y.$$

This is essentially a perturbation expansion; $u$ is a sum of $\delta$-functions to leading order, and $u_{reg}$ is a higher order correction. When the ansatz (6) is plugged into the system (5), the result is an equation for $u_{reg}$ which involves $\dot{x_j}(t)$. Imposing solvability conditions on this equation yields the following equation for $\dot{x_j}(t)$ to highest order:

$$\dot{x_j}(t) = -\frac{\Gamma(M_j(t))}{2\pi}\sum_{i \neq j} M_j(t)\frac{(x - x_i(t))}{|x - x_i(t)|^2} - \Gamma(M_j(t))\nabla_x v_{reg}(x_j(t),t),$$

where $\Gamma$ is a decreasing function with $0 < \Gamma(M) < 1$, $\lim_{M \to 8\pi^+} \Gamma(M) = 1$, and $\lim_{M \to \infty} = 0$. Matching conditions on outer and inner approximations yield the following equation for $\dot{M_j}(t)$:

$$\dot{M_j}(t) = u_{reg}(x_j(t),t) M_j(t).$$

Removing the small terms, i.e. those involving $u_{reg}$ and $v_{reg}$, we recover something like the point-particle dynamics analyzed below.

## 3. Results

3.1. **Our System.** For the purposes of this paper, we move from a continuum model of chemotaxis to a discrete model by imagining that our population density is the sum of $n$ of discrete populations, each at a location $x_j(t)$ with a total population of $m_j$, modeled by a $\delta$-function of the form $m_j\delta(x_j(t))$. Thus, the form of the population density $u$ is

$$u(x,t) = \sum_{j=1}^{n} m_j \delta(x_j(t)).$$

We use the simplified set of equations

$$\dot{x_j}(t) = \nabla c,$$
$$c_t = \Delta c + u.$$

If the rate at which diffusion happens is much faster than the rate at which the amoeba move, we can assume that $c$ reaches equilibrium instantaneously, and our equation for $c$ reduces to Poisson's equation with $u$ as a forcing term. Using Green's functions, we can solve for the acrasin density as

$$c(x,t) = -\frac{1}{4\pi}\sum_{j=1}^{n} m_j \log|x - x_j|.$$

Thus, the velocity of each population is given by

$$\dot{x_j}(t) = -\frac{1}{4\pi}\sum_{i\neq j} \frac{m_i(x_j - x_i)}{|x_j - x_i|^2}.$$

3.2. **Numerical Results.** This system was simulated numerically using an adaptive time-step. Populations within $10^{-4}$ of each other were combined. That is, their masses were summed, and one of the particles was deleted from the system. The number of populations at each timestep, and the average distance between populations, was plotted against time.

Results for an initial set of populations uniformly distributed in space over a square domain are shown in Figure 1. The number of populations clearly scales linearly with time, and the distance between populations is constant relative to the number of populations. Partial explanations of these observations are given in Section 3.

In Figure 2 and Figure 3 results are plotted for two initial configurations of populations, one uniformly and one normally distributed over a square domain. Both systems contain the same number of populations and the same expected mass. Notice that the profiles in Figure 2 are almost identical on this logarithmic scale, showing that the evolution of the normally distributed system is identical to the evolution of the uniformly distributed system, but faster.

To see how population density affects the scaling of the system, I ran the simulation with a steadily increasing number of initial populations having the same total mass (Figure 4). Since the populations were uniformly distributed over the domain, the initial conditions with a larger number of initial populations also had a higher initial population density. The linear scaling of the number of populations persists, with the slope being proportional to initial population density.

Figure 5 shows results for populations distributed uniformly over a variety of different domain shapes. The total mass of these systems is identical, although the number of populations is not. The domain shapes include a square, a circle, and a variety of multi-lobed shapes whose boundaries are given by the polar equation $r(\theta) = |\cos^7(\frac{n}{2}\theta)| + 1$, where $n$ is the number of lobes. The shape for $n = 6$ is shown in Figure 5. The scaling of the system changes little with $n$, so only results for $n = 3$ are shown. It is obvious that the domain shape has only a slight effect on the way the number of populations scales with time.

3.3. **Scaling.** The linear dependence of the number of populations on time can be explained using informal scaling arguments. Let $D$ be average distance between masses, $M$ the average density of a mass, $N$ the total number of masses, and $\tau$ the average time until a collision. Then,

$$\dot{x_j} \approx M \sum_{i \neq j} \frac{(x_j - x_i)}{|x_j - x_i|^2} \approx \frac{M}{L},$$

$$M \approx \frac{1}{N},$$

$$\tau \approx \frac{L}{\bar{\dot{x_j}}}.$$

Since mass is conserved within the system,

$$M \approx \frac{1}{N},$$

and thus

$$\tau \approx \frac{L}{(LN)^{-1}} = L^2 N.$$

Now,

$$\frac{\dot{N}}{N} = -\tau^{-1} \approx -L^{-2} N^{-1}.$$

Assuming that $L$ is constant in time (an assumption supported by our numerics), we have

$$\dot{N} \approx -L^{-2},$$

which accords with our numerical results, since $L^{-1}$ scales with population density.

## 4. Discussion and Conclusions

The fact that the density of populations remains constant over the evolution of the system is not easily explained scaling arguments. The domain over which the populations is distributed shrinks as the system evolves, so all the distances between particles shrink over time. However, particles that are very close together collide and aggregate, so small distance terms are quickly removed from the average. One suggestion is that the timescale on which nearby masses aggregate and the timescale on which the region occupied by the masses shrinks are different. The fact that the density of the masses is constant may represent a balance between these two timescales.

Observing the evolution of a set of populations distributed over a square domain, it becomes apparent that the dynamics near the corners are very different from the dynamics elsewhwere. Populations near the corners move more slowly towards the center of the domain than populations elsewhere. As the system evolves, the corners become sharper, and the domain becomes a four-pointed star, and then an 'X'. A set of populations distributed over a circular domain behaves very differently; as the system evolves, the domain shrinks but maintains its circular shape.

This phenomena can perhaps be explained in the following way. Due to the fact that each population's influence on other populations is mediated by a logarithmic potential, we can imagine that each population feels a kind of averaged influence from all the other populations in the system.

This explains the tendency of the domain to shrink towards its center. The 'corner populations' may feel a smaller influence from the system, since their exposure to the other populations is over a smaller arc. This may account for their slower movement towards the center of the domain. If this is the case, then discontinuities in the domain boundary may be the key to understanding how that boundary evolves with time. There may also be a connection to Laplacian growth, where a given section of the boundary of a domain grows at a speed proportional to its curvature. The domain of a system of aggregating particles may undergo a kind of Laplacian growth in reverse, where the speed of shrinkage is proportional to the inverse of the curvature.

There are many other questions to be answered about this and similar systems. Exploring the evolution of the boundary is one direction for future research. Also, the simple model of biological aggregation explored in this paper also exhibits a kind of finite-time blowup. At the end of our simulations, all the mass of the system has aggregated into a single point population. It would be interesting to see how a regularizing factor like the $\Gamma(M)$ postulated by Velazquez changes the dynamics of the system. Finally, attempting to include a nonlinear diffusion term like that in [2] may prove fruitful.

I would like to thank Karl Glasner for his help.

## References

[1] Keller E.F. & Segel L.A. (1970) Initiation of slime mold aggregation viewed as an instability. *J. theor. Biol.* 26, pp.399-415.

[2] Topaz C.M., Bertozzi A.L., Lewis M.A. (2005) A nonlocal continuum model for biological aggregation. *Preprint.*

[3] Velazquez J.J.L. (2004) Point dynamics in a singular limit of the Keller-Segel model 1: motion of the concentration regions. *SIAM J. Appl. Math.* 64, pp.1198-1223.

[4] Velazquez J.J.L. (2004) Point dynamics in a singular limit of the Keller-Segel model 2: formation of the concentration regions. *SIAM J. Appl. Math.* 64, pp.1224-1248.

[5] Brenner M.P., Constantin P., Kadanoff L.P., Schenkel A., Venkataramani, S.C. (1999) Diffusion, attraction, and collapse. *Nonlinearity* 12, pp.1071-1098.

## 5. Appendix: Figures

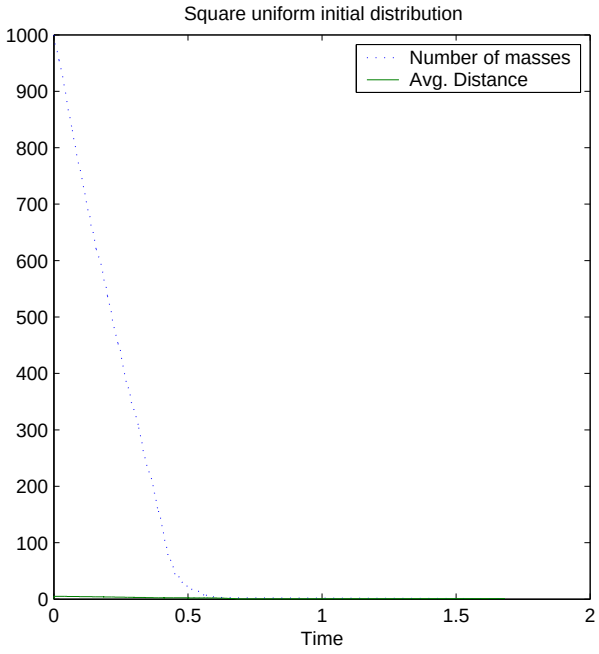


Figure 1. Number of masses and average distance against time for square, uniform distribution

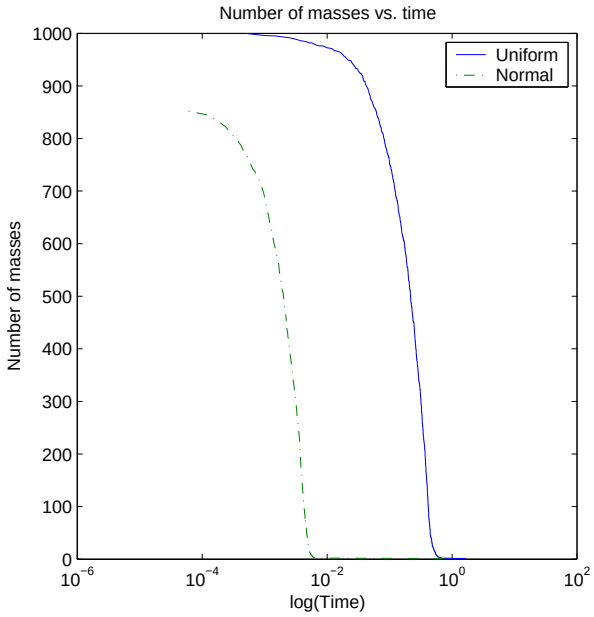


Figure 2. Number of masses for uniform vs. normal initial distributions of masses.

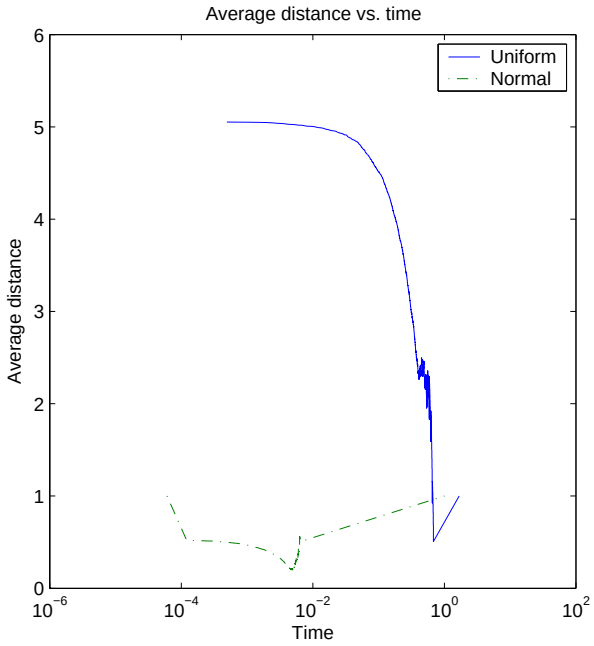


FIGURE 3. Average distance for uniform vs. normal initial distribution of masses.

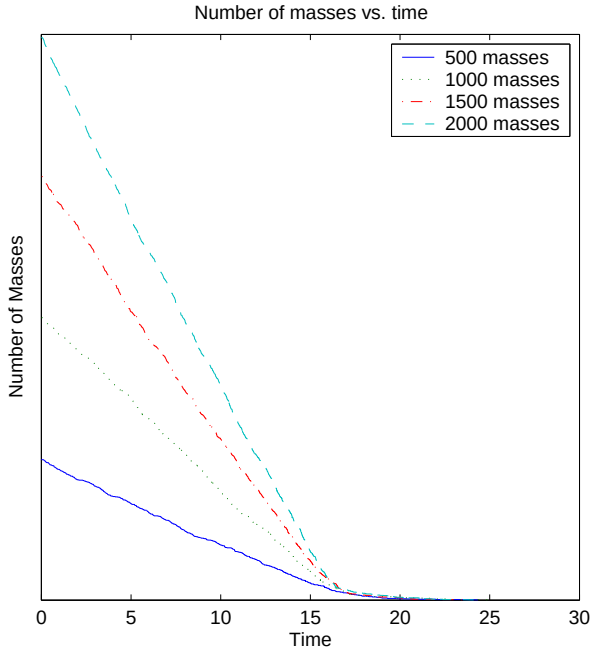


FIGURE 4. Number of masses and average distance against time for square, uniform distribution

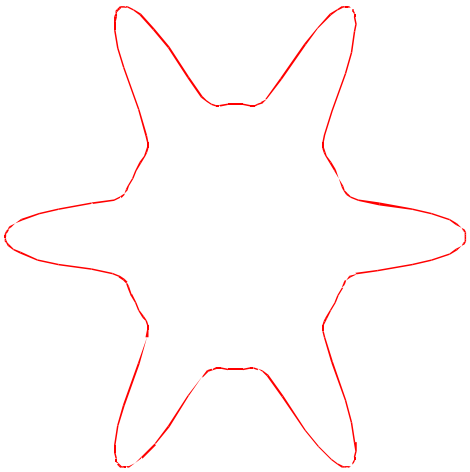

FIGURE 5. A 6-lobed domain shape.

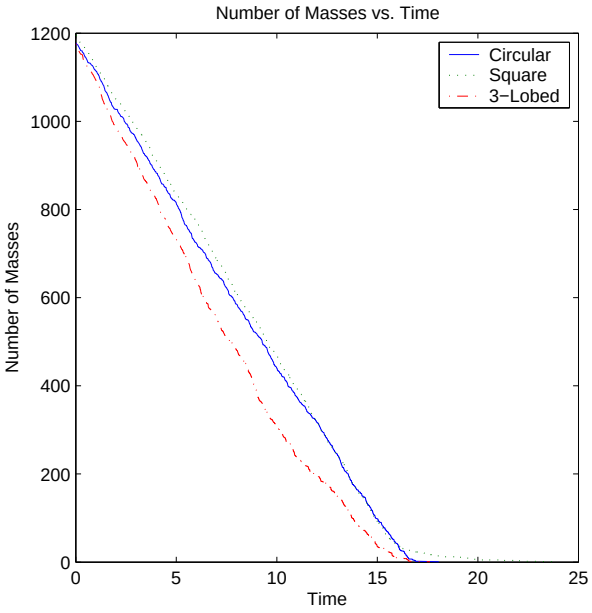


FIGURE 6. Number of masses for uniform distributions over various domains.